**ASMS**

RESEARCH ARTICLE

Mass Spectrometry Study of Multiply Negatively Charged, Gas-Phase NaAOT Micelles: How Does Charge State Affect Micellar Structure and Encapsulation?

Yigang Fang, Fangwei Liu, Jianbo Liu

Department of Chemistry and Biochemistry, Queens College and the Graduate Center of the City University of New York, 65-30 Kissena Blvd, Flushing, NY 11367, USA
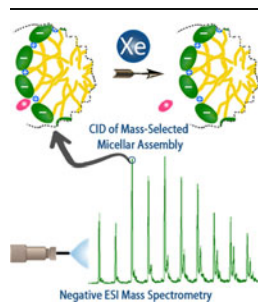
Abstract. We report the formation and characterization of multiply negatively charged sodium *bis*(2-ethylhexyl) sulfosuccinate (NaAOT) aggregates in the gas phase, by electrospray ionization of methanol/water solution of NaAOT followed by detection using a guided-ion-beam tandem mass spectrometer. Singly and doubly charged aggregates dominate the mass spectra with the compositions of $[Na_{n-z}AOT_n]^{z-}$ ($n=1$–18 and $z=1$–2). Solvation by water was detected only for small aggregates $[Na_{n-1}AOT_nH_2O]^-$ of $n=3$–9. Incorporation of glycine and tryptophan into $[Na_{n-z}AOT_n]^{z-}$ aggregates was achieved, aimed at identifying effects of guest molecule hydrophobicity on micellar solubilization. Only one glycine molecule could be incorporated into each $[Na_{n-z}AOT_n]^{z-}$ of $n \geq 7$, and at most two glycine molecules could be hosted in that of $n \geq 13$. In contrast to glycine, up to four tryptophan molecules could be accommodated within single aggregates of $n \geq 6$. However, deprotonation of tryptophan significantly decrease its affinity towards aggregates. Collision-induced dissociation (CID) was carried out for mass-selected aggregate ions, including measurements of product ion mass spectra for both empty and amino acid-containing aggregates. CID results provide a probe for aggregate structures, surfactant-solute interactions, and incorporation sites of amino acids. The present data was compared with mass spectrometry results of positively charged $[Na_{n+z}AOT_n]^{z+}$ aggregates. Contrary to their positive analogues, which form reverse micelles, negatively charged aggregates may adopt a direct micelle-like structure with AOT polar heads exposed and amino acids being adsorbed near the micellar outer surface.

Key words: Gas-phase micelles, NaAOT, Glycine, Tryptophan, Micellar incorporation, Collision-induced dissociation, Guided-ion-beam tandem mass spectrometry, Electrospray ionization

Introduction

Sodium *bis*(2-ethylhexyl)sulfosuccinate (NaAOT) is an ionic surfactant widely used in chemical and biophysical work for solubilization, separation, catalysis, drug delivery, nanoparticle synthesis, and generating membrane-mimetic systems [1–3]. It has two branched alkyl chains as shown in Figure 1, and is soluble in various solvents with the ability to assemble into direct or reverse micelles. When dissolved in polar solvents above its critical micellar concentration (CMC), NaAOT surfactants form direct micelles by hydrophobic effects, with their hydrophobic tails constituting an apolar center and hydrophilic polar heads in contact with surrounding solvent molecules [4–6], referred to as direct or "oil-in-water" micelles. By contrast, in nonpolar media [1, 6]

or super critical fluids [7], reverse micellar assemblies emerge with AOT polar heads oriented around an central core and hydrophobic chains directed outward. The size of reverse micelle grows by absorbing water into the inner core [3], and the system is described as "water-in-oil" microemulsion in the presence of a large water content.

An interesting question is whether direct and reverse micellar structures could evolve via self-assembling of NaAOT in the gas phase. In contrast with enormous work devoted to NaAOT aggregates in solution, only a handful of investigations have been reported concerning NaAOT aggregates as charged species in the gas phase [8–16], including electrospray ionization (ESI) and matrix-assisted laser desorption/ionization mass spectra [10, 14], time-of-flight secondary ion mass spectra [16] and infrared multiple photon dissociation spectra [13] of singly and doubly positively charged NaAOT aggregates. These measurements revealed reverse micelle-like structures for these aggregates.

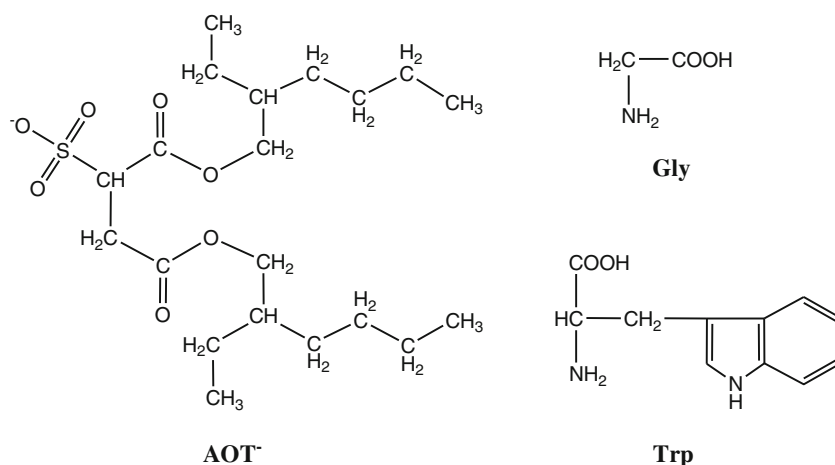*Correspondence to:* Jianbo Liu; *e-mail:* jianbo.liu@qc.cuny.edu

Figure 1.   Skeletal formulas of *bis*(2-ethylhexyl) sulfosuccinate anion (AOT⁻), Gly, and Trp

We have reported the formation of multiply positively charged NaAOT aggregates in the gas phase using ESI mass spectrometry, and have determined their structures using collision-induced dissociation (CID) [8]. These aggregates have the compositions of $[Na_{n+z}AOT_n]^{z+}$ with $z = 1$–5, and high charge states allow the detection of much larger aggregation numbers ($n = 2$–44) in the gas phase. Multiply charged $[Na_{n+z}AOT_n]^{z+}$ is able to accommodate guest molecules. Analysis of CID product ions and cross sections of glycine(Gly)-entrapping aggregates revealed that Gly is encapsulated within a hydrophilic core. We therefore concluded that $[Na_{n+z}AOT_n]^{z+}$ self-assembles into a multiply charged reverse micelle in the gas phase, with an inner core composed of hydrophilic polar head groups and counterions, and hydrophobic alkyl tails protruding into the vacuum. Parallel to experimental advances, molecular dynamics (MD) simulations have demonstrated that NaAOT reverse micelle remains stable *in vacuo* [17–19], with apolar tails collapsing on the outer surface to make the structure more compact [17].

More recently we have examined encapsulation of different amino acids into gas-phase $[Na_{n+z}AOT_n]^{z+}$ reverse micelles [9]. We found that integration into gas-phase reverse micelles depends upon amino acid hydrophobicity and charge states. For example, Gly and protonated tryptophan (TrpH⁺) are encapsulated within the micellar core; while neutral tryptophan (Trp) is intercalated at the micellar interface between surfactants. Therefore, gas-phase positively charged reverse micelles present similar encapsulation behaviors as their solution-phase counterparts [20–28]. Unlike their counterparts in solution, gas-phase reverse micelles have no inter-micelle exchange of solutes. As a result, they may protect micellar complexes during the transition from solution to the gas phase [29], function as nano-reactors to probe chemistry of guest molecules confined in or bound to gas-phase membrane mimetic systems, and allow for specialized measurements which have to be performed *in vacuo* (e.g., mass spectrometry and single-particle imaging [30]). Formation of gas-phase aggregates is

accompanied with solvent evaporation. Elimination of solvents removes surfactant–solvent interactions, but the electrostatics between surfactant polar heads and their counterions remains. From this perspective, gas-phase aggregates provide a simplified system for better understanding the roles of surfactant-surfactant and surfactant–counterion interactions in their self-assembling and entrapping of guest molecules [15].

In the present study, we extended our investigation to multiply negatively charged NaAOT micelles in the gas phase, attempting to ascertain whether or not charge state affects gas-phase micellar structure as well as micellar incorporation capability towards amino acids. A guided-ion-beam tandem mass spectrometer, coupled with an ESI source, was employed to examine the stoichiometry, incorporation, and dissociation of negatively charged aggregates. Our results lead to taking into consideration the possibility of a direct micelle-like structure for negatively charged gas-phase NaAOT aggregates.

Materials and Methods

NaAOT ($C_{20}H_{37}NaO_7S$, molecular weight 444.56, >99.0 %) was purchased from Fluka (St. Louis, MO, USA) and stored over P_2O_5 in a desiccator. Gly ($\geq$99 %) and L-Trp (99 %) were obtained from Sigma Aldrich (St. Louis, MO, USA). HPLC grade methanol and water, and reagent grade NaOH were obtained from Fisher Chemicals (Thermo Fisher Scientific, Waltham, MA, USA). Chemicals were used without further purification. ESI solutions were prepared in methanol/water (vol/vol = 1:1) containing NaAOT with concentration varying from 1.0×10^{-3} to 15×10^{-3} M. For amino acid-containing solution, 2.0×10^{-3} M Gly or Trp was added to methanol/water solution of 10×10^{-3} M NaAOT. To assist deprotonation of Trp, 10×10^{-3} M NaOH was added to the NaAOT/Trp solution. All solutions were sonicated for 10 min to help desolvation and degassing before ESI.

Mass spectra were acquired on a home-made guided-ion-beam tandem mass spectrometer described in detail previ-

ously [8, 9, 31–34]. The apparatus consists of an ESI [35, 36] ion source, radio frequency (rf) hexapole ion guide [37], quadrupole mass filter, rf octopole ion guide surrounded by a scattering cell, second quadrupole mass filter, and a detector. In the present study, the apparatus was operated in negative ion mode. Both quadrupole mass filters use Extrel 9.5 mm tri-filter rods, and were operated at 880 kHz to cover a mass/charge (m/z) range from 10 to 4,000. The mass resolving power was adjusted to over 100 to resolve the charge and stoichiometry of ions without significantly losing ion intensities.

Sample solutions were sprayed into ambient atmosphere through an electrospray needle at a flow rate (0.03 or 0.04 ml h^{-1}) optimized for each solution concentration. The electrospray needle was prepared in house [8, 9, 31–34], and biased at −1,900 to −2,400 V relative to ground. Negatively charged droplets formed from ESI were fed into a heated desolvation capillary assembly. The capillary was held at −200 V relative to ground and heated to 150 °C. Charged liquid droplets underwent desolvation as they passed through the heated capillary, converting to gas-phase negatively charged aggregates. A skimmer with an orifice of 0.99 mm (Beam Dynamics, Jacksonville, FL, USA) is located 3 mm from the capillary end, separating the ion source chamber and the hexapole ion guide. The skimmer was biased at −25 V relative to ground, and the electrical field imposed between the capillary and the skimmer removed remaining solvent molecules via collision-induced desolvation. After traveling through the skimmer, aggregate ions were transported into a rf hexapole ion guide at a pressure of 15–24 mTorr and underwent collisional cooling and focusing [38–40]. Focused ions passed into the first quadrupole for mass selection.

Mass-selected ions were injected into an rf octopole ion. The octopole ion guide was operated at 2.6 MHz with a peak-to-peak amplitude of 700 V. DC bias voltage was applied to the ion guide with its amplitude varying from −500 to +500 V. This DC bias voltage was used in retarding potential analysis [41] to determine the initial kinetic energy of mass-selected ions (i.e., intensities of ions were measured while sweeping the octopole bias. The DC bias voltage also allowed control of the kinetic energy of mass-selected ions in the laboratory frame. The kinetic energy (E_{lab}) of ions in the lab frame is then converted to the collision energy (E_{col}) between ions and neutral gas molecules in the center-of-mass frame using $E_{col} = E_{lab} \times m_{neutral}/(M_{ion} + m_{neutral})$, where $m_{neutral}$ and M_{ion} are masses of neutral collision gas and ions, respectively [42]. Note that for given octopole rf frequency (f) and amplitude (V_{rf}), only ions with radial velocities up to the well-defined cutoff values can be confined by the octopole [37]. At high E_{col}, light product ions may have high radial velocities. In order for these ions to have stable trajectories, the rf frequency should be large enough that the field changes polarity frequently on the time scale of the ions' radial motion within the octopole. On the

other hand, the magnitude of the effective potential (U_{eff}) confining the ions' radial motion is proportional to V_{rf}/mf^2. High frequency dictates high V_{rf}; however, there are V_{rf} limits set by arcing, and high V_{rf} also tends to exacerbate the breakdown of adiabaticity [37]. Given the large mass ratios of heavy ions to light neutral gas in this experiment, we varied E_{col} modestly from 0.5 to 2.0 eV for CID experiments, and observed similar fragmentation patterns of selected precursor aggregate ions. In the paper, we report CID mass spectra of mass-selected aggregates at $E_{col}=1.0$ eV, which allows direct comparison with CID results of positively charged aggregates obtained at the same E_{col} [8, 9].

The octopole runs through a scattering cell filled with collision gas Xe (99.995 %, Spectra Gases, Stewartsville, NJ, USA). The scattering cell pressure was controlled using a leak valve and measured by a Baratron capacitance manometer (MKS model 690 head and 670 signal conditioner, MKS Instruments, Andover, MA, USA). Due to low intensities of selected precursor ions, the cell pressure was set at 0.3 mTorr to achieve a good signal-to-noise ratio for product ions. However, precursor aggregate ions and product ions underwent multiple collisions at this pressure, making it impossible to determine cross sections for individual dissociation channels. Precursor aggregate ions and fragment ions were collected by the octopole ion guide, and directed to the second quadrupole for mass analysis. Ion signals were counted using a pulse-counting electron multiplier (DeTech model 411, Detector Technology, Palmer, MA, USA).

For conventional mass spectral measurements, the first quadrupole was rendered to an rf-only ion guide. In this arrangement, negatively charged aggregates generated from the ion source transmitted through the first quadrupole and were mass-scanned by the second quadrupole.

Results and Discussion

Formation of Multiply Negatively Charged NaAOT Aggregates

To investigate the effects of ESI solution conditions on the size, charge, and intensity distributions of gas-phase NaAOT aggregates, we measured mass spectra for a range of solutions with NaAOT concentration varying from 1.0×10^{-3} (below CMC of 2.5×10^{-3} M in aqueous solution [4]) to 15×10^{-3} M. Despite a wide variation in solution concentration, the abundance profiles of negatively charged gas-phase aggregates are nearly identical under all conditions, except that the absolute intensities of all aggregates increase significantly when a high concentration was used. When NaAOT concentration exceeded 15×10^{-3} M, a progressively growing background started to become significant; in the meantime, the absolute intensities of major peaks remained the same. Based on the quality of spectra, 10×10^{-3} M was chosen as the optimal concentration for all other experi-
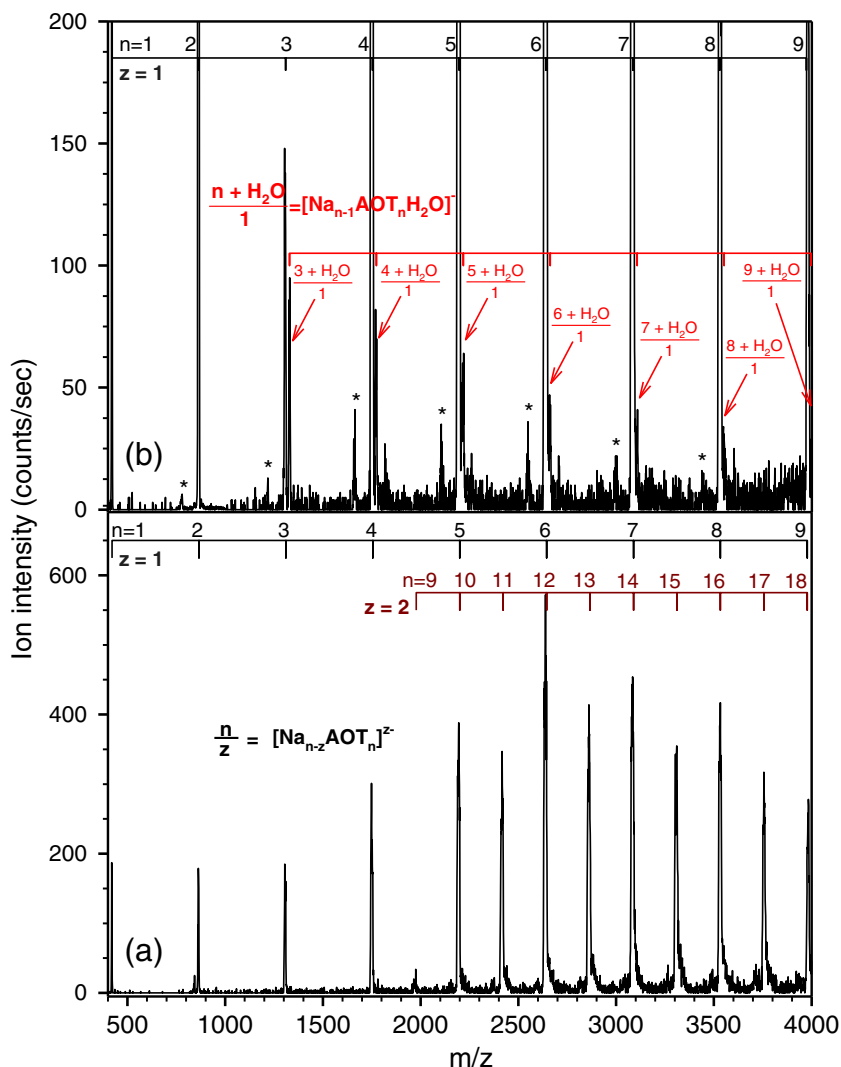
Figure 2. Negative ESI mass spectra of a methanol/water solution of 10×10^{-3} M NaAOT. Voltages applied to the capillary and the skimmer are (**a**) –200 V and –25 V, and (**b**) –300 V and –58 V, respectively. The features noted with '*' are due to fragmentation clusters, as explained in the text

ments. The mass spectrum obtained at this concentration is demonstrated in Figure 2a.

It is noteworthy that we observed a similar phenomenon concerning ESI solution conditions in a previous study of positively charged NaAOT aggregates in the gas phase [8]. In that experiment, we varied NaAOT concentration in methanol/water from 0.7×10^{-3} to 5.0×10^{-3} M to bracket the CMC. No difference was found in the size and charge distributions of resulting $[Na_{n+z}AOT_n]^{z+}$ aggregates, no matter whether or not the solution had a concentration above the CMC. Therefore, in both positive and negative ion modes, NaAOT concentration does not affect the evolution of gas-phase aggregates. It follows that, ESI mass spectra do not mirror NaAOT aggregation states in solution [14]; instead, aggregation of NaAOT takes place between ESI and exposure to the high vacuum of the mass spectrometer.

The mass peaks observed in Figure 2a can be attributed to the compositions of $[Na_{n-z}AOT_n]^{z-}$ with the aggregation number $n = 1 – 18$ and negative charge $z = 1 – 2$. In the figure,

the progressions of the same charge numbers are grouped together. For convenience, aggregates are indicated as n/z in the following discussion. Each aggregate lacks one to two Na^+ counterions, which accounts for its overall charge number. Singly charged aggregates start with monomer AOT^-, while doubly charged aggregates emerge from the aggregation number of 9. Relative abundance of singly charged aggregates (after subtracting the share of doubly charged species at the same m/z position) increases gradually till the maximum at 4/1, and then decreases. Doubly charged species exhibit a similar profile of ion intensity vs. aggregation number with a maximum intensity at 13/2; however, doubly charged species bear much higher intensities than neighboring singly charged ones. The actual maximum aggregation number for charged aggregates could be larger, since the largest detected aggregation number for each progression (i.e., 9 for $z = 1$ and 18 for $z = 2$) has approached the m/z detection limit of mass filters. However, "undetected" large aggregates would be less likely

to have high abundance based on the ion intensity profiles depicted in Figure 2a.

We note that NaAOT aggregates could only hold at most two extra charges in negative ion mode, much less than the extra charges they are able to carry in positive ion mode (i.e., $z=1–5$ for $[Na_{n+z}AOT_n]^{z+}$ [8]. This may imply a different way in which Coulomb repulsion affects the stability of negatively charged aggregates compared to their positively charged analogues, which in turn limits the size of aggregates in negative ion mode.

Our negative ESI mass spectra of NaAOT aggregates show some differences than those reported by Bongiorno et al. [10] and Giorgi et al. [12]. Although solutions were prepared in a similar manner, their negative ESI mass spectra correspond to only monocharged $[Na_{n-1}AOT_n]^-$, which parallels monocharged $[Na_{n+1}AOT_n]^+$ in their positive ESI mass spectra. We have detected multiply charged species in both positive [8] and negative ion modes. In our mass spectra, 4/1 exhibits the highest abundance among negatively monocharged species, while in theirs the monomer 1/1 is the most intense peak followed by the dimer 2/1. These discrepancies are most likely related to the differences in ESI and instrument conditions which were factored into the interactions of gas-phase surfactants and hence the distributions of gas-phase aggregates [8]. For these reasons, we collected all experimental date under nearly identical conditions, unless specified otherwise.

Solvation of Small Negatively Monocharged NaAOT Aggregates

Similar to the absence of water/methanol molecules in gas-phase positively charged $[Na_{n+z}AOT_n]^{z+}$ aggregates [8], solvent molecules were usually excluded in negatively charged aggregates, yielding "dry" $[Na_{n-z}AOT_n]^{z-}$ in Figure 2a. This provides further evidence that surfactant-surfactant interactions are an overwhelming driving force for self-assembling of NaAOT in the gas phase [15]. Solvent molecules are not necessary for building a large gas-phase aggregate architecture [8], neither are they required for entrapping guest molecules (*vide infra*). In fact, while solvation of small gas-phase AOT-divalent metal ion clusters has been recently detected [43], such as solvated monomeric aggregates $[MgAOT(CH_3OH)_2]^+$, $[MgAOT(CH_3OH)H_2O]^+$, and $[CaAOT(CH_3OH)]^+$, and dimeric aggregate $[NiAOT_2(CH_3OH)]^+$, solvated NaAOT aggregates has not been reported yet.

In the experiment, we found that among instrument operating parameters, the capillary-skimmer potential is most critical for the intensity and size distributions of aggregate ions. We, therefore, carried out a control experiment under the same condition as used for Figure 2a except that we increased the voltages applied on the capillary and skimmer to −300 V and −58 V, respectively. In this case, only monocharged aggregates $[Na_{n-1}AOT_n]^-$ of $n=1–9$ were detected (Figure 2b). This phenomenon can be attributed to the fact that multiply charged species are more sensitive to the capillary-skimmer potential. They gain higher translation energy than singly charged species

in the same electrical field, and thus cannot survive in-source CID. Similar results were observed in positive ESI mass spectra of NaAOT aggregates [8]. Accordingly, the high electrical field between the capillary and skimmer is unfavorable for aggregation and micellation. Interestingly, only under this high electrical field a new series of clusters emerges which can be assigned to solvation of aggregates by single water molecules, i.e.$[Na_{n-1}AOT_nH_2O]^-$ ($n=3–9$) as indicated in Figure 2b. The intensities of solvated aggregates are less than 5 % of corresponding "dry" aggregates, monotonously decreasing with increasing aggregate size. When pure methanol was used as the ESI solvent, these solvated aggregates mostly disappeared. Therefore, our results complement the observation of water solvated NaAOT aggregates in the gas phase. In addition to $[Na_{n-1}AOT_nH_2O]^-$, another series of low intensity aggregates were observed (marked with asterisks in Figure 2b). It starts at m/z of 778, and neighboring peaks differ by the number of NaAOT unit. We tentatively attribute this series to either an impurity present in NaAOT, or fragment ions formed during in-source collisions of "dry" aggregates.

Incorporation of Amino Acids within Negatively Charged NaAOT Aggregates

Neutral Gly Gly was chosen as the first guest molecule for the incorporation experiment, since a simple amino acid without a side chain would facilitate identification of key factors in gas-phase micellar entrapment. In this experiment, NaAOT solution was prepared in methanol/water, into which Gly was added ($[NaAOT]=10.0\times10^{-3}$M and $[Gly]=2.0\times10^{-3}$M). The negative ESI mass spectrum of NaAOT/Gly solution is shown in Figure 3. The most intense ion peaks in the mass spectrum have been assigned to empty aggregates n/z, and their abundance features are similar to those observed in Figure 2a. In the m/z range below 2000, mass spectrum of NaAOT/Gly is indistinguishable from that of pure NaAOT, suggesting that in this m/z range gas-phase aggregates are unoccupied. Occupied aggre-
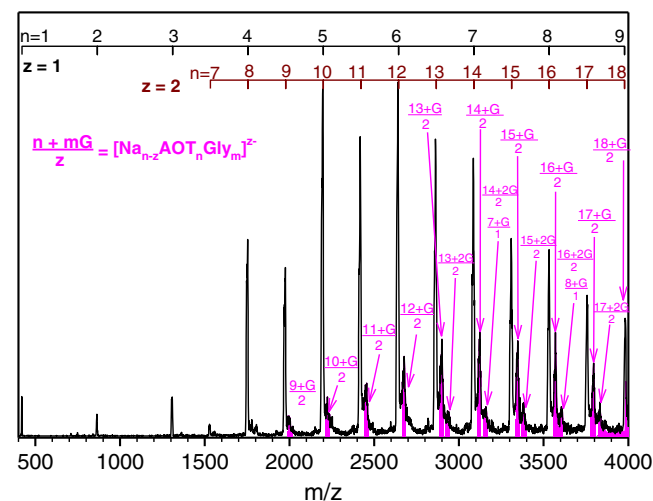

Figure 3. Negative ESI mass spectrum of a methanol/water solution containing 10×10^{-3}M NaAOT and 2.0×10^{-3}M Gly

gates are observed in the m/z range above 2000, featuring the compositions of $[Na_{n-z}AOT_nGly_m]^{z-}$ where m is the number of Gly molecules entrapped. These species are highlighted in pink in the figure, and labeled as $(n+mG)/z$. Note that there is m/z coincidence between singly and doubly charged species, for example, $(7+G)/1$ and $(14+2G)/2$; for these species both assignments are given. It was found that the entrapment capability of aggregates strongly correlates with their sizes. No entrapment of Gly was detected for aggregates with n less than 7. Aggregates of $n{\geq}7$ may accommodate single Gly, and up to two Gly molecules can be accommodated in aggregates of $n{\geq}13$.

Neutral Trp The Trp side chain (i.e., indole ring) is the most hydrophobic of all amino acid side chains, and aqueous solubility of Trp is 1.38 g/100 g water at 25 °C (compared with 25.16 g/100 g water for Gly) [44, 45]. Comparison of neutral Gly and Trp as guest molecules would allow for examination of hydrophobic effects in gas-phase micellar solubilization, and similar approaches have been used to determine the driving forces for the solubilization of amino acids in solution-phase NaAOT reverse micelles [20–23]. Negative mass spectrum of NaAOT/Trp was measured using a solution of NaAOT ($10{\times}10^{-3}$ M) and Trp ($2{\times}10^{-3}$ M) in methanol/water. pH of this solution was measured to be 6.5,

slightly higher than Trp isoelectric point pI of 5.9 in aqueous solution [46]. As shown in Figure 4a, neutral Trp was incorporated into $[Na_{n-z}AOT_n]^{z-}$ to form $[Na_{n-z}AOT_nTrp_m]^{z-}$ where m is the number of Trp entrapped. They are labeled as $(n+mW)/z$ in the figure, where W designates Trp. For the sake of clarity in showing the assignments of $(n+mW)/z$, the m/z range below 1400 is not shown in the figure, since no Trp signal was discernible in that range. In contrast to its low incorporation capability for Gly, each aggregate can entrap up to four Trp molecules, and there is no obvious correlation between aggregate size and the maximum number of Trp molecules each aggregate may host. In the figure all empty and Trp-entrapping aggregates associated with the same aggregate number are linked together, and aggregates with various values of m are shaded in different colors.

To quantitatively compare incorporation capability of the same aggregate towards Gly and Trp, we calculated relative incorporation efficiencies defined as

$$E_G = \frac{I([Na_{n-z}AOT_nGly]^{z-})}{I([Na_{n-z}AOT_n]^{z-})} \quad (1)$$

$$E_W = \frac{I([Na_{n-z}AOT_nTrp]^{z-})}{I([Na_{n-z}AOT_n]^{z-})} \quad (2)$$
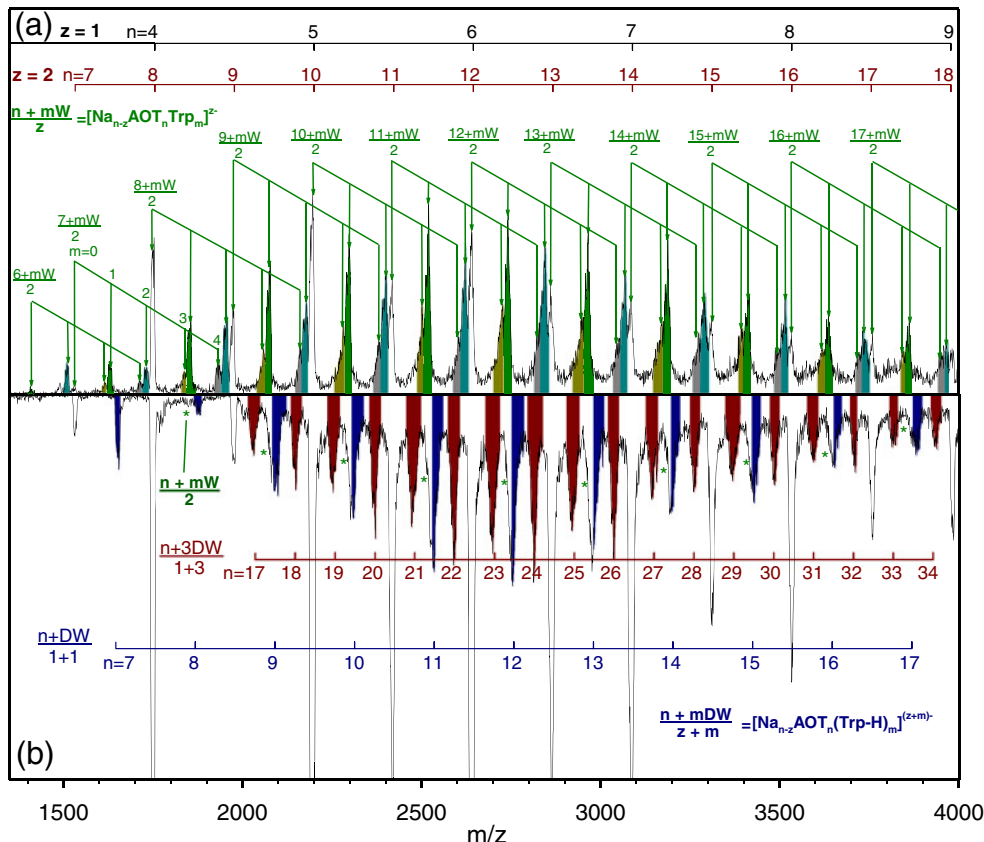
Figure 4. Negative ESI mass spectra of a methanol/water solution containing (**a**) $10{\times}10^{-3}$ M NaAOT and $2.0{\times}10^{-3}$ M Trp, and (**b**) $10{\times}10^{-3}$ M NaAOT, $2.0{\times}10^{-3}$ M Trp, and $10{\times}10^{-3}$ M NaOH

where $I([Na_{n-z}AOT_n]^{z-})$, $I([Na_{n-z}AOT_nGly]^{z-})$, and $I([Na_{n-z}AOT_nTrp]^{z-})$ represent ion intensities of empty aggregates and aggregates containing Gly and Trp, respectively, in corresponding mass spectra.

One issue in mass spectral measurements is that there are m/z coincidences among different charged states. Intensities of singly charged aggregate ions are masked by the shares of doubly charged ions at the same m/z positions. For example, m/z of 2644 represents two overlapping charge states, 6/1 and 12/2. To avoid complication arising from m/z coincidence of selected host aggregate ions with other charge states, we chose $[Na_{n-z}AOT_n]^{z-}$ of 7/2, 9/2, 11/2, 13/2, 15/2, and 17/2 as hosts for analysis. $[Na_{n-z}AOT_n]^{z-}$ may each incorporate more than one Gly and Trp molecule; however, incorporation of multiple Gly or Trp was not included in E_G or E_W. This omission was deliberate, since small $[Na_{n-z}AOT_n]^{z-}$ can only take one Gly each. To enable direct comparison of incorporation efficiencies of different aggregate sizes and towards different amino acids, we chose to focus on incorporation of single amino acid. Calculation results, averaged over at least two replicate sets of mass spectra, are summarized in Table 1. These results give very rough estimates, but are sufficient to reveal general trends.

Remarkable differences between values of E_G and E_W arise from distinct electrostatic and hydrophobic interactions involved in amino acid incorporation. For Gly, there is no hydrophobic interaction and an attractive electrostatic potential is essential for its solubilization into aggregates. Trp, in contrast, is the most hydrophobic amino acid [44, 45]. As shown by the ratios of E_W/E_G listed in Table 1, hydrophobicity dramatically increases the incorporation of Trp into aggregates by a factor of 9–14. But the enhancement decreases rapidly with increasing aggregate size, and approaches a minimum for aggregate of 17/2.

Deprotonated Trp Solubilization of neutral Trp can be attributed to hydrophobic effects. To distinguish the roles of hydrophobic and electrostatic interactions in micellar solubilization of the same amino acid, we adjusted pH of the NaAOT/Trp solution to 11.74 by adding 10×10^{-3} M NaOH. Under this

circumstance, deprotonated Trp was carried into negatively charged aggregates. The resulting spectrum (Figure 4b) has notable differences than that of neutral Trp (Figure 4a). Similar to that of NaAOT/Gly, this mass spectrum is overwhelmingly dominated by empty aggregates. In addition, two series of $[Na_{n-z}AOT_n(Trp-H)_m]^{(z+m)-}$ aggregates are identified, corresponding to aggregates containing single and three deprotonated Trp (hereafter designated as DW), respectively. These two series are indicated in dark blue and red shaded areas in Figure 4b, and labeled as $(n + DW)/(1 + 1)$ where n=7–17 and $(n+3DW)/1+3$ where n=17–34, respectively. It is somewhat puzzling that no aggregates containing two DW were detected. Note that $(n+DW)/(1+1)$ is partially overlapping with $(n + W)/2$ (which are marked with green asterisks in Figure 4b) because of the ionization equilibrium between deprotonated and neutral Trp in ESI solution and spray droplets.

We did not compare the relative incorporation efficiencies for deprotonated Trp with those for neutral Gly and Trp, since incorporation of deprotonated Trp happens only for monocharged $[Na_{n-1}AOT_n]^-$. However, deprotonation of Trp significantly reduces its incorporation into aggregates, making it resemble Gly in terms of incorporation efficiencies. This reduction may be rationalized by the displacement of Trp from the interfacial region close to apolar tails to the place near polar heads/counterions upon deprotonation. This implies that while hydrophobic effects between Trp side chain and surfactant apolar tails dominate Trp incorporation, these effects are compromised by electrostatics between Trp charged backbone and surfactant polar heads.

Comparison with Encapsulation Properties of Positively Charged Aggregates It is informative to compare the entrapment properties of negatively charged NaAOT aggregates with those of positively charged $[Na_{n+z}AOT_n]^{z+}$ reverse micelles we reported previously [8, 9]. $[Na_{n+z}AOT_n]^{z+}$ starts encapsulation of a Gly molecule from n=13, and those of $n \geq 16$ can encapsulate two Gly molecules. Up to three Gly molecules can be encapsulated in single $[Na_{n+z}AOT_n]^{z+}$ of $n \geq 17$, four Gly molecules in those of $n \geq 21$, and five in those of $n \geq 24$. This strong size dependence of encapsulation capability supports a reverse micelle-like structure for $[Na_{n+z}AOT_n]^{z+}$. Assuming $[Na_{n+z}AOT_n]^{z+}$ is spherical and Gly molecules are all encapsulated within the micellar core, the maximum number of encapsulated Gly molecules does indeed match the core size of the reverse micelle. On the other hand, incorporation of neutral Trp into $[Na_{n+z}AOT_n]^{z+}$ starts from n=10, and each $[Na_{n+z}AOT_n]^{z+}$ reverse micelle could only take at most one neutral Trp molecule. In line with a reverse micellar structure, Trp is interpreted to be intercalated between AOT tails at the reverse micellar interface. Small $[Na_{n+z}AOT_n]^{z+}$ reverse micelles have large curvatures and, consequently, cannot provide enough interfacial area (near head regions) for incorporating more than one Trp molecule.

The surprise is that the negative charge state of NaAOT aggregates dramatically affects their incorporation behaviors

Table 1. Incorporation efficiencies of Gly (G) and Trp (W) in gas-phase negatively (and positively) charged NaAOT aggregates

Negative host aggregates[a]	E_G[b]	E_W[b]	E_W/E_G[b]
$\frac{7}{2}$	-	5.6	-
$\frac{9}{2}$	0.12	1.7	14
$\frac{11}{2}$	0.18	1.6	9
$\frac{13}{2}$	0.33 (0.60)	1.5 (0.34)	4.5 (0.57)
$\frac{15}{2}$	0.48 (0.90)	1.3 (0.62)	2.7 (0.69)
$\frac{17}{2}$	0.54 (1.50)	1.2 (0.70)	2.2 (0.47)

[a]Host aggregates are indicated as $\frac{n}{z}$, where n is the aggregation number, and z is the total charge
[b]Values in parentheses are incorporation efficiencies of Gly and Trp in positively charged aggregates, and their ratios, respectively

towards Gly *vs.* Trp, yielding distinctly different results. $[Na_{n-z}AOT_n]^{z-}$ requires lower aggregation number to entrap Gly molecules; on the other hand, incorporation of more than two Gly molecules was not observed in single $[Na_{n-z}AOT_n]^{z-}$. Moreover, each $[Na_{n-z}AOT_n]^{z-}$ can entrap four neutral Trp molecules, and the efficiency for incorporating the second Trp molecule is comparable to that for the first one. For comparison, we have included in Table 1 the incorporation efficiencies for Gly and Trp in positively charged NaAOT aggregates, respectively [8, 9]. It is obvious that $[Na_{n+z}AOT_n]^{z+}$ and $[Na_{n-z}AOT_n]^{z-}$ present opposite affinities towards hydrophilic Gly and hydrophobic Trp, as exemplified by the values of E_G/E_W for corresponding positively and negatively charged aggregates. This gives us a hint that $[Na_{n+z}AOT_n]^{z+}$ and $[Na_{n-z}AOT_n]^{z-}$ may have different mechanisms to accommodate guest molecules.

CID of Negatively Charged NaAOT Aggregates

Empty Aggregates Four doubly charged aggregates with odd aggregation numbers (i.e., 11/2, 13/2, 15/2, and 17/2) were chosen as precursor ions for CID experiments. Each of these precursor ions could be cleanly mass-selected and corresponds to a unique aggregation number, circumventing the complications of *m/z* coincidences with other species. CID mass spectra described below were obtained at $E_{col}=$ 1.0 eV and with 0.3 mTorr Xe in the scattering cell. The values of E_{col} and cell pressure are the same as those used for positively charged aggregates in a previous study [8, 9], so that the results from two different charge states can be compared.

Figure 5 shows the product ion mass spectra from CID of mass-selected precursor ions. Because of multiple collisions between precursor ions and Xe at a high gas pressure (and primary fragment ions may continue to undergo collisions that cause secondary dissociations), relative intensities of product ions in the spectra do not reflect branching ratios. However, all product ions in Figure 5 were detected under single-collision condition as well.

Dissociation product ions for all selected precursor ions are summarized in Table 2. Also included in the table are dissociation efficiencies (*Diss%*), estimated as

$Diss\% =$

$$\frac{\Sigma\, I(\text{monocharged fragment ion})/2}{\Sigma\, I(\text{monocharged fragment ion})/2 + I(\text{doubly charged precursor ion})}$$
(3)

for each precursor ion. CID of doubly charged precursor ions exclusively produces two monocharged species. Unless otherwise stated, both complementary product ions, produced from a single dissociation of a doubly charged precursor ion, were detected and are included in
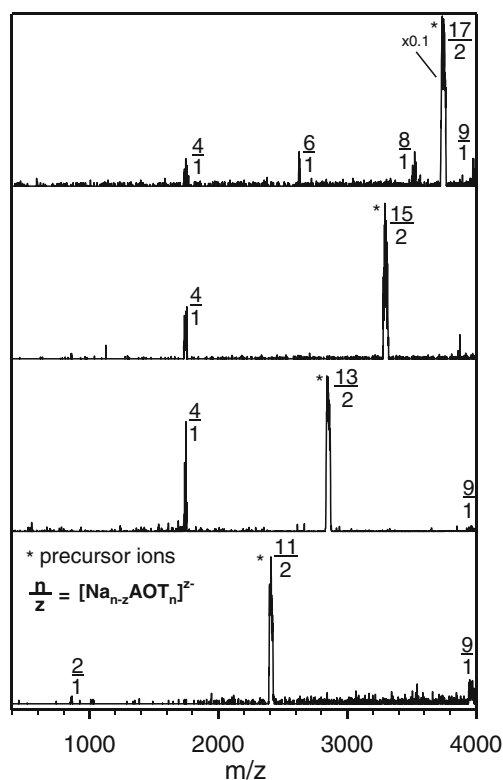

Figure 5. CID mass spectra of mass-selected negatively charged NaAOT aggregates. Spectra were measured at $E_{col}=$ 1.0 eV, with 0.3 mTorr Xe in the scattering cell. Asterisks indicate precursor ions

the table. Some fragment ion peaks may be attributed to more than one product ion because of the overlapping of singly and doubly charged species. However, based on the trend in product ion charge state distributions, the contributions of doubly charged product ions are less likely to be significant. Most precursor ions have only one dissociation channel, except the largest one, 17/2, which dissociates into 4/1+13/1, 6/1+11/1, and 8/1+9/1, respectively. Dissociation efficiency strongly depends on the aggregate size, increasing from 9 % for 11/2 to 25 %–26 % for 13/2 and 15/2, and dropping to only 5 % for 17/2, suggesting the exceptionally high stability of 17/2.

Aggregates Containing Gly and Trp Different than that of empty aggregates, CID of aggregates containing guest molecules involves a competition between stripping surfactants and expelling entrapped guest molecules. Such competition is driven by precursor ion structures and the stability of resulting neutral and charged products [8, 9]. To enable a direct comparison with empty aggregates, we selected Gly and Trp-containing precursor aggregates with the same aggregation and charge numbers as those chosen for empty aggregates (i.e., (11+G or W)/2, (13+G or W)/2, (15+G or W)/2, and (17+G or W)/2).

Figure 6a and b show CID mass spectra of negatively charged NaAOT aggregates containing Gly and Trp, respectively. These mass spectra clearly reveal that there exists only one dissociation channel for each of these precursor aggregate ions, which corresponds to striping of Gly (or Trp), and only Gly (or Trp), off aggregates. This indicates that both Gly and Trp may be attached to the exterior of aggregate structures. As opposed to being encapsulated within the aggregate core, an amino acid anchored onto the outer surface could be easily knocked off by Xe collision without collapse of the remaining aggregate.

We have also compared dissociation efficiencies for aggregates containing Gly and Trp. As summarized in Table 2, for both systems the dissociation efficiency increases with the aggregate size, except for $(13+G)/2$, which presents an abnormally high dissociation efficiency. Under the same CID conditions, the dissociation efficiencies for aggregates containing Gly are higher than those containing Trp by a factor of 3–5 or more. In fact, Trp-containing aggregates have dissociation efficiencies more or less comparable to empty aggregates. This result is in agreement with what we have learned from incorporation efficiencies (Table 1), and reinforces that hydrophobic Trp has a higher affinity to NaAOT surfactants than hydrophilic Gly.

CID of aggregates containing deprotonated Trp could be another ideal system for probing entrapment properties of negatively charged 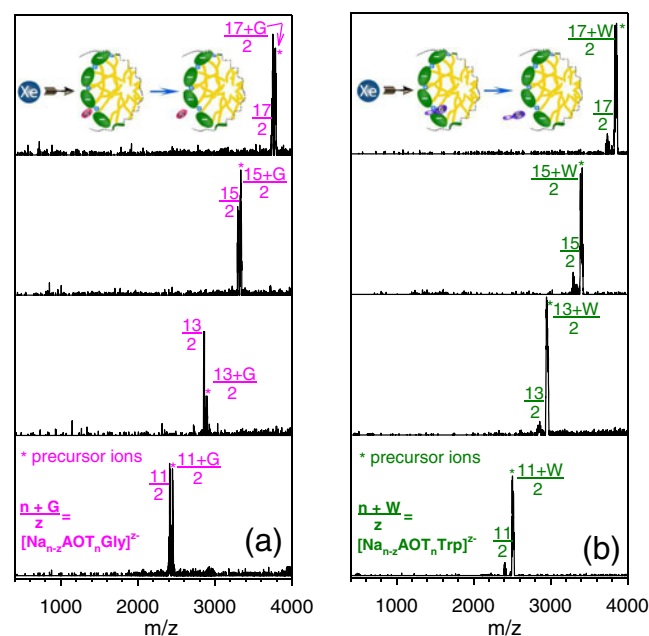aggregates, because deprotonated Trp combines hydrophobic side chain and charged hydrophilic backbone. Unfortunately, NaAOT aggregates containing deprotonated Trp coexist and overlap with aggregates containing neutral Trp in mass spectra, which prevented us to select "clean" deprotonated Trp-containing precursor ions for CID.

Comparison with CID of Positively Charged Aggregates We first compare CID products of positively and negatively charged empty aggregates of the same size. To differentiate the charge state for the same aggregation number, we include the sign of charge in the superscript of the acronym, e.g., n/z^+ for $[Na_{n+z}AOT_n]^{z+}$ and n/z^- for $[Na_{n-z}AOT_n]^{z-}$. We reported that the major CID channels of $[Na_{n+2}AOT_n]^{2+}$ correspond to divisions of the precursor ion into two nearly equally-sized monocharged product ions [8], referred to as "symmetric fission" [47]. For instances, $13/2^+ \rightarrow 6/1^+ + 7/1^+$, $15/2^+ \rightarrow 7/1^+ + 8/1^+$, and $17/2^+ \rightarrow 8/1^+ + 9/1^+$. On the contrary, the sizes of two fragment ions produced from a $[Na_{n-2}AOT_n]^{2-}$ aggregate differ greatly (i.e., asymmetric division to one larger and one smaller species) such as $13/2^- \rightarrow 4/1^- + 9/1^-$, $15/2^- \rightarrow 4/1^- + 11/1^-$, and $17/2^- \rightarrow 6/1^- + 11/1^-$.

It is more instructive to compare CID of amino acid-containing NaAOT aggregates in different charge states. The most profound difference is found in Gly-containing aggregates. Dissociation of positively charged Gly-containing aggregates produces various product ions, some of which remain entrapping Gly. This has been taken as a strong piece of evidence that Gly is protected within the interior of a reverse micelle. By contrast, for negatively charged aggregates, only Gly is eliminated without losing NaAOT units. CID of Trp-containing NaAOT aggregates goes to another extreme, where all occupied aggregates expel Trp only, regardless of aggregate charge states.

What Structure May Gas-Phase Negatively Charged NaAOT Aggregates Possess?

Before analyzing what mass spectrometry study tells us about the structure of negatively charged NaAOT aggregates, it is useful to stress the differences emerging from a comparative analysis of negatively charged $[Na_{n-z}AOT_z]^{z-}$ and positively charged $[Na_{n+z}AOT_z]^{z+}$, the latter forming reverse micelle in the gas phase [8, 9]. The main points are: (1) $[Na_{n+z}AOT_z]^{z+}$ reverse micellar ions can accommodate up to five extra charges, whereas $[Na_{n-z}AOT_z]^{z-}$ aggregates can only hold two extra charges; (2) $[Na_{n+z}AOT_z]^{z+}$ ions show a high encapsulation capability towards hydrophilic Gly with a strong size dependence, yet a limited incorporation capability towards hydrophobic Trp. $[Na_{n-z}AOT_z]^{z-}$ aggregates present opposite behaviors, showing a much higher entrapping capability towards Trp (without aggregate size dependence) than towards Gly; (3) protonation of Trp significantly improves its incorporation into $[Na_{n+z}AOT_z]^{z+}$ as it displaces Trp from the micellar interfacial zone to the core, whereas deprotonation of Trp dramatically decreases its incorporation into $[Na_{n-z}AOT_z]^{z-}$;

Figure 6. CID mass spectra of mass-selected negatively charged NaAOT aggregates containing (**a**) Gly and (**b**) Trp. All spectra were measured at E_{col}=1.0 eV, with 0.3 mTorr Xe in the scattering cell. Asterisks indicate precursor ions. Inserted cartoons illustrate (**a**) adsorption of Gly near surfactant polar heads and (**b**) interfacial incorporation of Trp as a co-surfactant, respectively

Table 2. Summary of CID Products And Dissociation Efficiencies of Empty and Amino Acid-Containing Negatively Charged NaAOT Aggregates

Empty precursor ions[a]	Dissociation channels[b]	Precursor ions containing Gly[a]	Dissociation channels[b]	Precursor ions containing Trp[a]	Dissociation channels[b]
$\frac{11}{1}$	$\frac{2}{1}+\frac{9}{1}\,(9\%)$	$\frac{11+G}{2}$	$\frac{11}{2}+G\,(51\%)$	$\frac{11+W}{2}$	$\frac{11}{2}+W\,(10\%)$
$\frac{13}{2}$	$\frac{4}{1}+\frac{9}{1}\,(26\%)$	$\frac{13+G}{2}$	$\frac{13}{2}+G\,(73\%)$	$\frac{13+W}{2}$	$\frac{13}{2}+W\,(7\%)$
$\frac{15}{2}$	$\frac{4}{1}+\frac{11^c}{1}\,(25\%)$	$\frac{15+G}{2}$	$\frac{15}{2}+G\,(42\%)$	$\frac{15+W}{2}$	$\frac{15}{2}+W\,(15\%)$
$\frac{17}{2}$	$\frac{8}{1}+\frac{9}{1}$	$\frac{17+G}{2}$	$\frac{17}{2}+G\,(53\%)$	$\frac{17+W}{2}$	$\frac{17}{2}+W\,(10\%)$
	$\frac{6}{1}+\frac{11^c}{1}$				
	$\frac{4}{1}+\frac{13^c}{1}$				
	(total 5 %)				

[a]Precursor and fragment ions are indicated as $\frac{n}{z}$ for empty aggregates, $\frac{n+mG}{z}$ for those containing Gly (G), and $\frac{n+mW}{z}$ for those containing Trp (W), where n is the aggregation number, z is the total charge, and m is the number of incorporated amino acid molecules.

[b]Given in parentheses are the dissociation efficiencies, estimated as $\dfrac{\sum I(\text{monocharged fragment ion})/2}{\sum I(\text{monocharged fragment ion})/2+I(\text{doubly charged precursor ion})}$ for empty aggregates, and $\dfrac{I(\text{fragment ion})}{I(\text{fragment ion})+I(\text{precursor ion})}$ for aggregates containing amino acid.

[c] Beyond the m/z detection limit of the mass spectrometer.

(4) CID of $[\text{Na}_{n+z}\text{AOT}_z\text{Gly}]^{z+}$ leads to various fragments, and expelling of Gly results in breakdown of the micellar structure. CID of $[\text{Na}_{n+z}\text{AOT}_z\text{Trp}]^{z+}$, on the other hand, corresponds to striping only Trp off reverse micelles. We attributed these CID patterns to different site locations of amino acids within reverse micelles, i.e., Gly is encapsulated into the micellar core, whereas Trp is intercalated at the micellar interface. Conversely, for CID of negatively charged aggregates containing Gly and Trp, the above described difference vanishes — at the same E_{col} used for positively charged reverse micelles both Gly- and Trp-containing negatively charged aggregates eject only amino acid. These dissimilarities indicate that different from what is expected for reverse micellar incorporation, both Gly and Trp are loosely attached to negatively charged micelles.

These discrepancies lead to clues regarding possible $[\text{Na}_{n-z}\text{AOT}_z]^{z-}$ structures in the gas phase. Bongiorno et al. [10, 48] and Giorgi et al. [12] reported gas-phase negatively monocharged NaAOT aggregates. Bongiorno et al. calculated the energy changes accompanying the formation of reverse and direct micelles for neutral, positively and negatively singly charged AOT trimers and found the electrostatic interactions among surfactant head groups are larger than apolar–apolar interactions among surfactant alkyl chains, which would favor a reverse micellar model for these trimers. MD simulations [18] suggest positively and negatively singly charged and neutral NaAOT aggregates may all form reverse micelle-like structures; however, a negatively charged aggregate is the least stable and has larger total gyration radius (including all atoms) and core gyration radius (including core atoms only) than the same size neutral and positively charged aggregates, which implies additional repulsive effect for a negatively charged aggregate if existing in a reverse micellar structure.

Compared with singly charged aggregates, multiply charged aggregates bring about more intense Coulombic repulsion. One way towards understanding the structures of

multiply charged aggregates is to identify different effects of extra positive and negative charges. The presence of Na^+ counterions in the $[\text{Na}_{n+z}\text{AOT}_z]^{z+}$ reverse micelle allows the repulsive interaction of AOT negative polar heads to be overcome; and extra Na^+ ions improve this gluing effect. This scenario raises a related question. Would multiply charged $[\text{Na}_{n+z}\text{AOT}_z]^{z+}$ be destabilized because of Coulombic repulsion when Na^+ ions are too close to each other? Based on a direct optimization of dry, isolated NaAOT reverse micelles [17] and MD simulations of low water content NaAOT reverse micelles in isooctane [49, 50], most Na^+ ions penetrate the layer of AOT polar heads and coordinate with the sulfonate group. Some Na^+ ions exist outside and coordinate with the carbonyl group. Coordination of Na^+ with these oxygen atoms offers a favorable structure for $[\text{Na}_{n+z}\text{AOT}_z]^{z+}$. On the other hand, had $[\text{Na}_{n-z}\text{AOT}_z]^{z-}$ adopted a similar reverse micellar structure as $[\text{Na}_{n+z}\text{AOT}_z]^{z+}$, repulsive interactions among "unneutralized" AOT^- polar heads (localized in the micellar center) could not be "shielded" from each other. This would have induced inherent instability, leading to disruption of the whole micellar structures.

Based on these considerations and our incorporation and CID results, we propose that a direct micelle-like model (which exposes polar heads) might better describe the structures and encapsulation properties of multiply negatively charged aggregates than a reverse micelle-like model (with polar heads buried within the interior of the micelle). In a direct micelle-like structure, Gly may adsorb to the interface through electrostatics with NaAOT polar heads and counterions; Trp, due to its hydrophobic indole ring, may partially penetrate into the surfactant layer. The cartoons in Figure 6a and b illustrate direct micelle-like structures for Gly- and Trp-containing aggregates. These cartoons are not intended to describe the whole structures of respective aggregates, but to demonstrate the localization of Gly and Trp and how these guest amino acids were facilely eliminated during CID. A direct micelle-like

structure explains our observation that $[Na_{n-z}AOT_z]^{z-}$ aggregates have a higher affinity towards Trp than towards Gly. Following the principle of "like dissolves like," Trp could penetrate into AOT apolar tails acting as a co-surfactant and consequently gain more space compared to Gly. It follows that Trp incorporation shows weak aggregate size dependence. Furthermore, deprotonation of Trp introduces repulsion between Trp charged backbone and AOT polar head. This electrostatic tends to push Trp away from the micellar surface, leading to reduced incorporation efficiency. Finally, the fact that Xe collision could strip Gly or Trp off the host without breaking the host structure is consistent with location of guest molecule near the exposed layer of a direct micelle-like structure. As Trp side chain and AOT tails coalesce into a more stable architecture, less fragmentation would be expected for aggregates containing Trp. We note that in addition to spherical direct micelle, other structures such as helicoidal or rodlike micelle [51] with exposed polar heads may also be in agreement with encapsulation and dissociation behaviors of NaAOT aggregates. However, a helicoidal or rodlike micelle with replicate structure units along one dimension cannot explain the fact that while hydrophobic effects increase the incorporation of Trp into aggregates, the enhancement decreases rapidly with increasing aggregate size (Table 1).

We note that gas-phase direct micelles have been reported for other systems, e.g., 3-[(3-cholamidopropyl)-dimethylammonio]-1-propanesulfonate (CHAPS) [52], sodium dodecylsulfate (SDS) [52], bile salt [53], and decyltrimethylammonium bromide (DTAB) [54]. Particularly, Robinson et al. reported formation of gas-phase direct and reverse micelles using different ESI solutions of cetyltrimethylammonium bromide (CTAB) [51].

Conclusions

The present experimental study ascertains that NaAOT surfactants can form multiply negatively charged micelles in the gas phase with compositions of $[Na_{n-z}AOT_n]^{z-}$ where $n=1$–18 and $z=1$–2. Micellation occurs via self-assembling of surfactants in the gas phase, and does not mirror aggregation states in ESI solutions. Solvation is only detected for small, negatively charged aggregates, indicating that solvent–surfactant interactions are not essential for the formation of micelles in the gas phase. Incorporation of Gly, neutral and deprotonated Trp into $[Na_{n-z}AOT_n]^{z-}$ was achieved, respectively. Incorporation of hydrophilic Gly shows strong aggregate size dependence. $[Na_{n-z}AOT_n]^{z-}$ of $n \geq 7$ could incorporate one Gly molecule, and those of $n \geq 13$ can incorporate two Gly molecules. For comparison, $[Na_{n-z}AOT_n]^{z-}$ shows a much higher incorporation capability towards hydrophobic Trp and could accommodate up to four Trp molecules each from the size of $n=6$. However, deprotonation significantly reduces Trp incorporation. Collision-induced dissociation of negatively charged empty aggregates and those containing Gly and Trp was carried out. Fragmentation results were utilized to infer micellar ion structures and incorporation sites of amino acids and, hence, to propose a direct micelle-like structure for these assemblies. These findings are different from those of positively charged NaAOT aggregates which have been proved to take a reverse micelle-like structure. It demonstrates that micelles formed from the same solution but under different charge states exhibit markedly different mass spectra. More importantly, different charge states might affect resulting micellar structures, and consequently their incorporation behaviors.

Acknowledgments

References

1. Luisi, P.L., Giomini, M., Pileni, M.P., Robinson, B.H.: Reverse micelles as hosts for proteins and small molecules. *Biochim. Biophys. Acta* **947**, 209–246 (1988)
2. Kon-no, K.: Properties and applications of reversed micelles. *Surf. Colloid Sci.* **15**, 125–151 (1993)
3. Pileni, M.-P.: The role of soft colloidal templates in controlling the size and shape of inorganic nanocrystals. *Nat. Mater.* **2**, 145–150 (2003)
4. Williams, E.F., Woodbery, N.T., Dixon, J.K.: Purification and surface-tension properties of alkyl sodium sulfosuccinates. *J. Colloid Interface Sci.* **12**, 452–459 (1957)
5. Mukerjee, P.; Mysels, K. J. *Critical Micelle Concentration of Aqueous Surfactant Systems*; NSRDC-NBS 36: Washington, DC, (1971).
6. Mukherjee, K., Moulik, S.P., Mukherjee, D.C.: Thermodynamics of micellization of aerosol OT in Polar and nonpolar solvents. A calorimetric study. *Langmuir* **9**, 1727–1730 (1993)
7. Gale, R.W., Fulton, J.L., Smith, R.D.: Organized molecular assemblies in the gas phase: reverse micelles and microemulsions in supercritical fluids. *J. Am. Chem. Soc.* **109**, 920–921 (1987)
8. Fang, Y., Bennett, A., Liu, J.: Multiply charged gas-phase NaAOT reverse micelles: formation, encapsulation and collision-induced dissociation. *Int. J. Mass Spectrom.* **293**, 12–22 (2010)
9. Fang, Y., Bennett, A., Liu, J.: Selective transport of amino acids into the gas phase: driving forces for amino acid solubilization in gas-phase reverse micelles. *Phys. Chem. Chem. Phys.* **13**, 1466–1478 (2011)
10. Bongiorno, D., Ceraulo, L., Ruggirello, A., Turco Liveri, V., Basso, E., Seraglia, R., Traldi, P.: Surfactant self-assembling in gas phase: electrospray ionization- and matrix-assisted laser desorption/ionization-mass spectrometry of singly charged AOT clusters. *J. Mass Spectrom.* **40**, 1618–1625 (2005)
11. Giorgi, G., Ceraulo, L., Turco Liveri, V.: surfactant self-assembly in the gas phase: *bis*(2-ethylhexyl)sulfosuccinate-alkaline metal ion aggregates. *J. Phys. Chem. B* **112**, 1376–1382 (2008)
12. Giorgi, G., Giocaliere, E., Ceraulo, L., Ruggirello, A., Turco Liveri, V.: Spatially ordered surfactant assemblies in the gas phase: negatively charged *bis*(2-ethylhexyl)sulfosuccinate alkaline metal ion aggregates. *Rapid Comm. Mass Spectrom.* **23**, 2206–2212 (2009)
13. Giorgi, G., Ceraulo, L., Berden, G., Oomens, J., Turco Liveri, V.: Gas phase infrared multiple photon dissociation spectra of positively charged sodium *bis*(2-ethylhexyl)sulfosuccinate reverse micelle-like aggregates. *J. Phys. Chem. B* **115**, 2282–2286 (2011)
14. Bongiorno, D., Ceraulo, L., Giorgi, G., Indelicato, S., Turco Liveri, V.: Do Electrospray mass spectra of surfactants mirror their aggregation state in solution? *J. Mass Spectrom.* **46**, 1263–1268 (2011)

15. Ceraulo, L., Giorgi, G., Turco Liveri, V., Bongiorno, D., Indelicato, S., Di Gaudio, F., Indelicato, S.: Mass spectrometry of surfactant aggregates. *Eur. J. Mass Spectrom.* **17**, 525–541 (2011)

16. Burns, S.A., Valint Jr., P.L., Gardella Jr., J.A.: Determination of critical micelle concentration of aerosol-OT using time-of-flight secondary ion mass spectrometry fragmentation ion patterns. *Langmuir* **25**, 11244–11249 (2009)

17. Bulavchenko, A.I., Batishchev, A.F., Batishcheva, E.K., Torgov, V.G.: Modeling of the electrostatic interaction of ions in dry, isolated micelles of AOT by the method of direct optimization. *J. Phys. Chem. B* **106**, 6381–6389 (2002)

18. Longhi, G., Fornili, S.L., Turco Liveri, V., Abbate, S., Rebeccani, D., Ceraulo, L., Gangemi, F.: Sodium *bis*(2-ethylhexyl)sulfosuccinate self-aggregation *in vacuo*: molecular dynamics simulation. *Phys. Chem. Chem. Phys.* **12**, 4694–4703 (2010)

19. Longhi, G., Abbate, S., Ceraulo, L., Ceselli, A., Fornili, S.L., Turco Liveri, V.: A molecular dynamics study of structure, stability and fragmentation patterns of sodium *bis*(2-ethylhexyl)sulfosuccinate positively charged aggregates *in vacuo*. *Phys. Chem. Chem. Phys.* **13**, 21423–21431 (2011)

20. Leodidis, E.B., Hatton, T.A.: Amino acids in AOT reversed micelles. 1. Determination of interfacial partition coefficients using the phase-transfer method. *J. Phys. Chem.* **94**, 6400–6411 (1990)

21. Leodidis, E.B., Hatton, T.A.: Amino acids in AOT reversed micelles. 2. The hydrophobic effect and hydrogen bonding as driving forces for interfacial solubilization. *J. Phys. Chem.* **94**, 6411–6420 (1990)

22. Leodidis, E.B., Bommarius, A.S., Hatton, T.A.: Amino acids in reversed micelles. 3. Dependence of the interfacial partition coefficient on excess phase salinity and interfacial curvature. *J. Phys. Chem.* **95**, 5943–5956 (1991)

23. Leodidis, E.B., Hatton, T.A.: Amino acids in reversed micelles. 4. Amino acids as cosurfactants. *J. Phys. Chem.* **95**, 5957–5965 (1991)

24. Leodidis, E.B., Hatton, T.A.: Effects of average molecualr charge on amino acid interfacial partitioning in reversed micelles. *J. Colloid Interface Sci.* **147**, 163–177 (1991)

25. Adachi, M., Harada, M., Shioi, A., Sato, Y.: Extraction of amino acids to microemulsion. *J. Phys. Chem.* **95**, 7925–7931 (1991)

26. Cardoso, M.M., Barradas, M.J., Carrondo, M.T., Kroner, K.H., Crespo, J.G.: Mechanisms of amino acid partitioning in cationic reversed micelles. *Bioseparation* **7**, 65–78 (1998)

27. Fu, X., Li, J., Ma, Y., Zhang, L., Wang, D., Hu, Z.: Amino acid extraction with AOT reverse micelle. *Colloid Surf. A* **179**, 1–10 (2001)

28. Rinaldi, R., Volpe, P.L.O., Torriani, I.L.: L-tryptophan transport through a hydrophobic liquid membrane using AOT micelles: dynamics of the process as revealed by small angle X-ray scattering. *J. Colloid Interface Sci.* **318**, 59–67 (2008)

29. Borysik, A.J., Robinson, C.V.: Formation and dissociation processes of gas-phase detergent micelles. *Langmuir* **28**, 7160–7167 (2012)

30. Neutze, R., Wouts, R., van der Spoel, D., Weckert, E., Hajdu, J.: Potential for biomolecular imaging with femtosecond X-ray pulses. *Nature* **406**, 752–757 (2000)

31. Fang, Y., Liu, J.: Reaction of protonated tyrosine with electronically excited singlet molecular oxygen: an experimental and trajectory study. *J. Phys. Chem. A* **113**, 11250–11261 (2009)

32. Fang, Y., Liu, F., Bennett, A., Ara, S., Liu, J.: Experimental and trajectory study on reaction of protonated methionine with electronically excited singlet molecular oxygen ($a^1\Delta_g$): reaction dynamics and collision energy effects. *J. Phys. Chem. B* **115**, 2671–2682 (2011)

33. Liu, F., Fang, Y., Chen, Y., Liu, J.: Dissociative excitation energy transfer in the reactions of protonated cysteine and tryptophan with electronically excited singlet molecular oxygen ($a^1\Delta_g$). *J. Phys. Chem. B* **115**, 9898–9909 (2011)

34. Liu, F., Fang, Y., Chen, Y., Liu, J.: Reactions of deprotonated tyrosine and tryptophan with electroniclaly excited singlet moleuclar oxygen ($a^1\Delta_g$): a guided-ion-beam scattering, statistical modeling, and trajectroy study. *J. Phys. Chem. B* **116**, 6369–6379 (2012)

35. Yamashita, M., Fenn, J.B.: Electrospray Ion Source. Another variation on the free-jet theme. *J. Phys. Chem.* **88**, 4451–4459 (1984)

36. Fenn, J.B., Mann, M., Meng, C.K., Wong, S.F., Whitehouse, C.M.: Electrospray ionization for mass spectrometry of large biomolecules. *Science* **246**, 64–71 (1989)

37. Gerlich, D.: Inhomogeneous rf fields: a versatile tool for the study of processes with slow ions. In: Ng, C.Y., Baer, M. (eds.) State-Selected and State-to-State Ion-Molecule Reaction Dynamics. Part I. Experiment, vol. 82, pp. 1–176. John Wiley and Sons, Inc, New York (1992)

38. Moision, R.M., Armentrout, P.B.: An electrospray ionization source for thermochemical investigation with the guided ion beam mass spectrometer. *J. Am. Soc. Mass Spectrom.* **18**, 1124–1134 (2007)

39. Krutchinsky, A.N., Chernushevich, I.V., Spicer, V.L., Ens, W., Standing, K.G.: Collisional damping interface for an electrospray ionization time-of-flight mass spectrometer. *J. Am. Soc. Mass Spectrom.* **9**, 569–579 (1998)

40. Douglas, D.J., French, J.B.: Collisional focusing effects in radio frequency quadrupoles. *J. Am. Mass Spectrom.* **3**, 398–408 (1992)

41. Ervin, K.M., Armentrout, P.B.: Translational energy dependence of $Ar^+ + XY \rightarrow ArX^+ + Y$ ($XY = H_2, D_2, HD$) from thermal to 30 eV c.m. *J. Chem. Phys.* **83**, 166–189 (1985)

42. Armentrout, P.B.: Fundamental of ion-molecule chemistry. *J. Anal. At. Spectrom.* **19**, 571–580 (2004)

43. Giorgi, G., Pini, I., Ceraulo, L., Liveri, V.T.: Gas phase charged aggregates of *bis*(2-ethylhexyl)sulfosuccinate (AOT) and divalent metal ions: first evidence of aot solvated aggregates. *J. Mass Spectrom.* **46**, 925–932 (2011)

44. Nozaki, Y., Tanford, C.: The solubility of amino acids and two glycine peptides in aqueous ethanol and dioxane solutions: establishment of a hydrophobicity scale. *J. Biol. Chem.* **246**, 2211–2217 (1971)

45. Wimley, W.C., White, S.H.: Experimentally determined hydrophobicity scale for proteins at membrane interfaces. *Nat. Struct. Biol.* **3**, 842–848 (1996)

46. Vollhardt, P., Schore, N.: Organic Chemistry, 6th edn. W. H. Freeman and Company, New York (2009)

47. Donaldson, D.J., Tuck, A.F., Vaida, V.: Spontaneous fission of atmospheric aerosol particles. *Phys. Chem. Chem. Phys.* **3**, 5270–5273 (2001)

48. Bongiorno, D., Ceraulo, L., Giorgi, G., Indelicato, S., Ferrugia, M., Ruggirello, A., Turco Liveri, V.: Effects of the net charge on abundance and stability of supramolecular surfactant aggregates in gas phase. *J. Mass Spectrom.* **46**, 195–201 (2011)

49. Faeder, J., Ladanyi, B.M.: Molecular dynamics simulations of the interior of aqueous reverse micelles. *J. Phys. Chem. B* **104**, 1033–1046 (2000)

50. Chowdhary, J., Ladanyi, B.M.: Molecular dynamics simulation of aerosol-OT reverse micelles. *J. Phys. Chem. B* **113**, 15029–15039 (2009)

51. Sharon, M., Ilag, L.L., Robinson, C.V.: Evidence for micellar structure in the gas phase. *J. Am. Chem. Soc.* **129**, 8740–8746 (2007)

52. Siuzdak, G., Bothner, B.: Gas-phase micelles. *Angew. Chem. Int. Ed.* **34**, 2053–2055 (1995)

53. Cacace, F., de Petris, G., Giglio, E., Punzo, F., Troiani, A.: Bile salt aggregates in the gas phase: an electrospray ionization mass spectrometric study. *Chem. Eur. J.* **8**, 1925–1933 (2002)

54. Nohara, D., Bitoh, M.: Observation of Micelle Solution of Decyltrimethylammonium Bromide by Electrospray Ionization Mass Spectrometry. *J. Mass Spectrom.* **35**, 1434–1437 (2000)